JPE 16-1-5

http://dx.doi.org/10.6113/JPE.2016.16.1.38
ISSN(Print): 1598-2092 / ISSN(Online): 2093-4718

A Droop Method for High Capacity Parallel Inverters Considering Accurate Real Power Sharing

Donghwan Kim*, Kyosun Jung*, Kyungbae Lim*, and Jaeho Choi†

†,*School of Electrical Engineering, Chungbuk National University, Cheongju, Korea

Abstract

This paper presents DG based droop controlled parallel inverter systems with virtual impedance considering the unequal resistive-inductive combined line impedance condition. This causes a reactive power sharing error and dynamic performance degradation. Each of these drawbacks can be solved by adding the feedforward term of each line impedance voltage drop or injecting the virtual inductor. However, if the line impedances are high enough because of the long distance between the DG and the PCC or if the capacity of the system is large so that the output current is very large, this leads to a high virtual inductor voltage drop which causes reductions of the output voltage and power. Therefore, the line impedance voltage drops and the virtual inductor and resistor voltage drop compensation methods have been considered to solve these problems. The proposed method has been verified in comparison with the conventional droop method through PSIM simulation and low-scale experimental results.

Key words: Droop control, parallel inverters, power sharing, virtual impedance, distributed generation (DG)

I. INTRODUCTION

Due to the demand for eco-friendly solutions and stable local power supplies, concerns about the DG (Distributed Generation) systems are growing due to the microgrid concept being increasingly considered as a local power supply network system [1]. A microgrid is an integration of RES (Renewable Energy Sources) such as the photovoltaic or wind power generators and fuel cell with an engine generator, batteries, etc. It has been issued due to its flexibility and capability as a reliable power supply. A microgrid is usually connected to the main grid by DG through parallel inverters located near the local loads. The flexible operation of a full system is possible because DG improves the accessibility of local loads and realizes the local control of DG. Therefore, microgrid differs from the centralized generation which is mainly composed of large-scale generation such as thermal power generation or nuclear power generation [2].

A DG based microgrid operates in either the grid-connected mode or the islanded mode [3]. In the grid-connected mode, a microgrid can be defined as a current source because it supplies power to the main grid by synchronizing the phase of the PCC (Point of Common Coupling) voltage. However, when a grid fault occurs or a strategic islanding is needed, it has to be transferred to the islanded mode by opening the static switch which connects the microgrid to the PCC. Then, the microgrid is defined as a voltage source because it can supply the full load demand with only the local DG units instead of the main grid. In the islanded mode, the DG based parallel inverters have to supply the high quality power and the full local load demands with load sharing among inverters [2].

One method for the load sharing of parallel inverters is the master-slave control [4], [5]. In this method, one voltage controlled inverter is operated as a master module and the other current controlled inverters are operated as slave modules. It is simple and shows very good performance in term of load sharing despite the unequal line impedances by the mutual communication among the inverters. However, its drawback becomes more serious when a control failure occurs in the master module. This is a problem because the control of the slave modules are mainly affected by the control of the master module due to the intercommunication line between master and slave inverters [4]. It can also cause a transient overcurrent problem due to communication delays.

Manuscript received Oct. 19, 2015; accepted Dec. 11, 2015
Recommended for publication by Associate Editor Il-Yop Chung.
†Corresponding Author: choi@cbnu.ac.kr
Tel: +82-43-261-2425, Fax: +82-43-276-7217 Chungbuk Nat'l Univ.
*School of Electrical Eng., Chungbuk National University, Korea

To overcome these problems, frequency and voltage droop control methods are usually used to realize the load sharing and to maintain the frequency and voltage of the PCC without communications among the parallel inverters [6]-[17]. In addition, this also guarantees reliable operation of the parallel inverters even under the DG unit's hot swap connection. However, the DG based droop controlled parallel inverter operation when the line impedances between the inverters and the PCC are unequal and when there are inductive-resistive combined lines, can cause a reactive power sharing error and a dynamic performance degradation due to the unequal line voltage drop and the PQ power coupling, respectively.

To reduce the reactive power sharing error and to avoid the mutual interference between P-Q and ω-E, several solutions have been proposed. In [6], the virtual power frame droop method has been used by transforming P and Q to virtual power through the R/X ratio of the line impedance to decouple the power coupling. In [7], the virtual frequency-voltage frame droop method has been used through the R/X ratio of the line impedance by the same token as the previous method. However, these two methods are limited because they need the same R/X ratio on each line impedance of DGs. In [9]-[17], the virtual impedance has been proposed to decouple the P-Q coupling by making the system overall impedance dominant. It has advantages in terms of decoupling the power without the same R/X ratio of line impedances among the DGs. In addition, to compensate the aforementioned reactive power sharing error due to the unequal line voltage drop, the feedforward term of the line voltage drop has been considered [2], [9]. In these approaches, the calculation of the line voltage drop is based on the power flow analysis according to the R and X values and the output power. Hence, the reactive power sharing error due to the unequal line voltage drops can be significantly reduced without using the high voltage droop coefficient. Note that a higher voltage droop coefficient realizes a faster dynamic and a more accurate power sharing. However, this can cause system instability due to the increase of the droop coefficient.

However, if the line impedances are high enough because of the long distance between the DG and the PCC or if the capacity of that system is large and the output current is very large, then it results in a high virtual inductor voltage drop which causes a reduction of the output voltage and power [11]. Note that the virtual impedance voltage drop is obtained through the multiplication of both the virtual impedance value and the output current [12]. Hence, the line impedance voltage drop and the virtual inductor voltage drop estimation have been considered in this paper. This paper shows that it is possible to adopt a selection method of the virtual impedance through small-signal modeling for the analysis of the transient state [13].

In addition, the case of injecting the virtual resistor which can achieve better performance under the condition of resistive line impedances has been considered so that each DG based parallel inverter operates within the range of its rated output voltage and power. The proposed method has been verified in comparison with the conventional droop method through PSIM and Matlab simulations and low-scale experimental results.

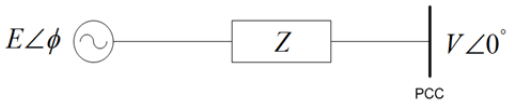

Fig. 1. Equivalent circuit of distributed generation system.

II. Droop Control and System Modeling

A. Conventional Droop Control

Fig. 1 shows an equivalent circuit of a distributed generation system. Based on this model, equations about both the real and reactive powers can be obtained for a DG system. The line impedance is represented as $\bar{Z} = Ze^{j\theta} = R + jX$. Then, the complex power which flows through the transmission line is as follows:

$$\begin{aligned}\bar{S} &= P + Q = \bar{V}\,\bar{\mathrm{I}}^{*} = V\left(\frac{E\angle\phi - V}{\bar{Z}}\right)^{*} \\ &= \frac{VE}{Z}e^{j(\theta-\phi)} - \frac{V^2}{Z}e^{-j\theta} \\ &= \frac{VE}{Z}(\cos(\theta-\phi) + j\sin(\theta-\phi)) - \frac{V^2}{Z}(\cos\theta - j\sin\theta)\end{aligned} \tag{1}$$

Here, $E\angle\phi$ is the output voltage of the distributed generation, $\bar{Z}$ is the impedance between the PCC and the DG system, and $\bar{V}$ is the PCC voltage. It is considered to be $\theta = 90°$ because the line impedance is assumed to be the dominant inductive component in the conventional droop method. The above equation can be simplified as follows:

$$P \cong \frac{VE}{X}\sin\phi \tag{2}$$

$$Q \cong \frac{V}{X}(E\cos\phi - V) \tag{3}$$

The phase of the PCC voltage ϕ can be assumed to be 0 because it is very small in practice. Hence, (2) and (3) can be simplified as follows:

$$\phi \approx \frac{XP}{EV}, \quad E - V \approx \frac{XQ}{V} \tag{4}$$

Equation (4) shows that the inverter phase and voltage are proportional to the real power and the reactive power, respectively. Note that controlling the angular frequency ω instead of controlling the phase ϕ has to be selected in the droop control for smoother transient dynamics and system stability. Finally, the $P-\omega$ and $Q-E$ droop control equations can be obtained as follows [6]:

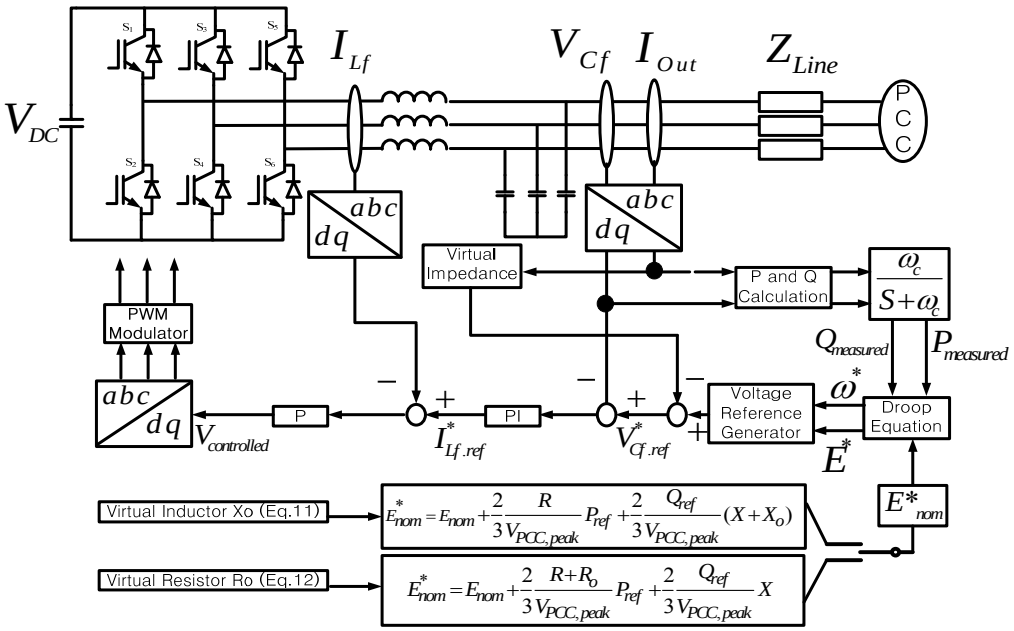

Fig. 2. Current voltage control scheme for distributed generation interfaced with inverter.

$$\omega^* = \omega_{nom} - k_\omega (P_{ref} - P) \quad (5)$$

$$E^* = E_{nom} - k_v (Q_{ref} - Q) \quad (6)$$

ω_{nom} : Nominal frequency

E_{nom} : Nominal voltage

ω^* : Reference frequency

E^* : Reference voltage

k_ω : Frequency-P droop coefficient

k_v : Voltage-Q droop coefficient

On the other hand, if the droop method adopts the predominant resistive line condition as the distribution line, the droop equations need to be changed to the following equations due to the different coupling between $P-\omega$ and $Q-E$.

$$\omega^* = \omega_{nom} + k_\omega (Q_{ref} - Q) \quad (7)$$

$$E^* = E_{nom} - k_v (P_{ref} - P) \quad (8)$$

B. System Modeling and Virtual Inductor Method

The conventional droop has been considered since the inductive component is dominant more than the resistive component in the line impedance. However, the line impedance in a real system sometimes contains a resistive component somewhat in accordance with the type of system. Hence, the mutual interference component occurs in the relation between the real and reactive power. The injection of the virtual inductance method to the inductive-resistive complex line reduces the mutual interference so that the conventional droop method can be more effective.

Fig. 2 represents the overall control scheme of the droop control in this paper. As shown in this figure, the inductor current and the filter capacitor voltage have been used as a feedback. Additionally, the output currents which flow through the line have also been used for the calculation of the output power and the voltage drop at the virtual impedance. The voltage and current controller is designed as PI-P controllers and their gains have been selected through the root-locus analysis with deliberation. However, the conventional virtual inductor voltage drop calculation with differentiation cannot be a good application because of the noise amplification due to the differentiation. Furthermore, this can be more serious when the inverter supplies power to non-linear loads. Therefore, avoiding high frequency problems by adding a high pass filter has been studied [12, 14]. However, it is not easy to select the filter cutoff frequency and it is complicated because this frequency should be changed according to the configuration of the system and load. Hence, this paper adopts a simple voltage drop calculation method of virtual impedance without differentiation by considering the complexity mentioned in [9].

$$(V_d + jV_q) = j\omega X_\circ \left(I_d + jI_q\right) = \omega X_\circ \left(-I_q + jI_d\right) \quad (9)$$

$X_\circ$: Virtual reactance

ω : System angular frequency

As shown in Fig. 3, the differentiation can be avoided by simplifying sX_o to $j\omega X_o$ for the calculation of the d- and q-components of the reactance voltage drop. Therefore, (9) which adopts the d-q synchronous reference frame improves the noise attenuation at high frequency. Figure 4 represents the virtual resistor implementation which gives more advantages under resistive predominant line impedance conditions such as a low voltage line cable. Note that using a

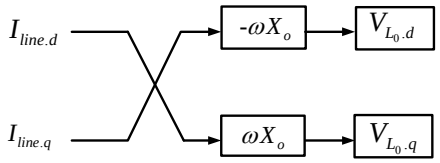

Fig. 3. Virtual inductor scheme without differentiation.

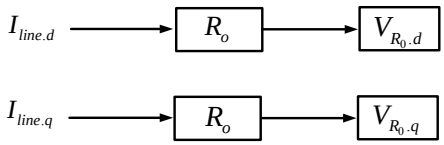

Fig. 4. Virtual resistor scheme.

virtual resistor is preferable to a virtual inductor in a predominantly resistive line, otherwise a larger virtual inductor is needed to be dominant when compared with the resistive component.

C. Proposed Active and Reactive Power Sharing

As mentioned in the introduction, a reactive power sharing error occurs due to the unequal voltage drops when the line impedances of parallel inverters are unbalanced. If the voltage droop coefficient is very large for compensating the reactive power error, then there may be an unstable transient response and steady-state oscillations. Note that although the ramp function can be used for improving the transient dynamics, the steady-state oscillation may still exist due to the high steady-state voltage droop coefficient.

In [9], the conventional droop method has been modified by using saved information which consists of both resistive and inductance components analyzed by changes of the real and reactive power in the grid-connected mode. However, this kind of analysis is quite complicate because it is difficult to know the effect the real and reactive power may have on the voltage drop at line impedances. Additionally, it may be necessary to use a low-pass filter for smoothening the measured real and reactive power. Therefore, in this paper, the impedance voltage drop is calculated by considering the islanded mode firstly. Then, the reference voltages are modified with these calculated variables. The modified reference voltage is given as (10).

$$E_{nom}^{*} = E_{nom} + \frac{2}{3}\frac{R}{V_{PCC,peak}}P_{ref} + \frac{2}{3}\frac{(X + X_o)}{V_{PCC,peak}}Q_{ref} \quad (10)$$

E_{nom}^{*} : Proposed rated voltage

$V_{PCC,peak}$: Peak value of the PCC rated voltage

By using (10), it is possible to realize the zero steady-state error of the reactive power and the transient load sharing performance of the real power. From (10), the voltage-reactive power droop equation can be obtained as (11).

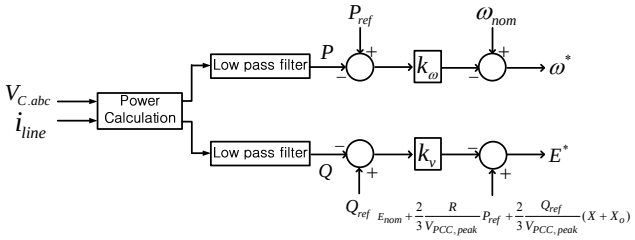

Fig. 5. Proposed droop algorithm for inductive line.

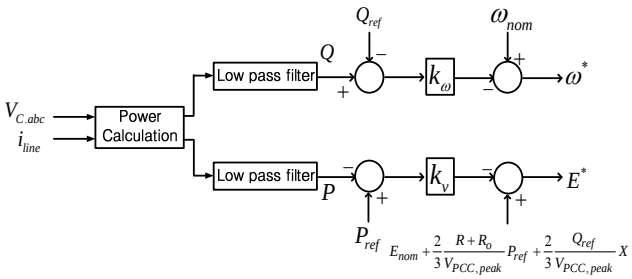

Fig. 6. Proposed droop algorithm for resistive line.

$$E_{ref}^{*} = E_{nom} + \frac{2}{3}\frac{R}{V_{PCC,peak}}P_{ref} + \frac{2}{3}\frac{(X + X_o)}{V_{PCC,peak}}Q_{ref} - k_v(Q_{ref} - Q) \quad (11)$$

The details of (11) are shown in Fig. 5. In a high capacity system, the output current which flows through the line is very large. Hence, it makes the voltage drop at the virtual inductance larger than the nominal voltage which causes an output power reduction due to the reference voltage reduction caused by the big virtual impedance voltage drop. Therefore, by using (10) and (11), it can be improved to achieve zero reactive power sharing error and the high performance of real power sharing. Additionally, when line impedances are predominantly resistive, the resistive droop equation can be considered as Fig. 6. With the conventional resistive droop, the opposite of reactive power sharing is correct but a real power sharing error occurs due to the unbalanced line impedance. As a result, the resistive droop equation is proposed as (12) as in (11).

$$E_{ref}^{*} = E_{nom} + \frac{2}{3}\frac{(R + R_o)}{V_{PCC,peak}}P_{ref} + \frac{2}{3}\frac{X}{V_{PCC,peak}}Q_{ref} - k_v(P_{ref} - P) \quad (12)$$

As shown in (12), the voltage-real power droop has been used and the voltage drops of both the line impedance and the virtual resistor have been considered to reduce the real power sharing error [16].

D. Small Signal Modeling and System Stability Analysis

The system stability can be analyzed by using the linearized equation of small signal modeling in the transient state [17]. The conventional droop control has treated small signal modeling without considering the virtual inductor. In this

paper, the virtual inductor has been considered in the small signal modeling and its validity has been checked through Matlab simulation as proposed in [13].

The DG output voltage E is defined as $e_d + je_q$, and the output current $i_d + ji_q$ is shown as (13).

$$i_d + ji_q = \frac{\bar{E} - \bar{V}}{\bar{Z}} = \frac{1}{Z}[(e_d - V)\cos\theta + e_q \sin\theta] - \frac{j}{Z}[(e_d - V)\sin\theta - e_q \cos\theta] \quad (13)$$

The small signal equation for the current can be obtained by the linearizing (13).

$$\triangle i_d = \frac{1}{Z}(\triangle e_d \cos\theta + \triangle e_q \sin\theta) \quad (14)$$

$$\triangle i_q = -\frac{1}{Z}(\triangle e_d \sin\theta - \triangle e_q \cos\theta) \quad (15)$$

Equation (14) can be obtained from (1) by transforming to the dq-synchronous reference frame.

$$p + jq = V(i_d + ji_q) = V \cdot i_d - jV \cdot i_q \quad (16)$$

By using (11), the linearized equation of (14) is given as following:

$$\triangle p = V\triangle i_d = \frac{V}{Z}(\triangle e_d \cos\theta + \triangle e_q \sin\theta) \quad (17)$$

$$\triangle q = -V\triangle i_q = \frac{V}{Z}(\triangle e_d \sin\theta - \triangle e_q \cos\theta) \quad (18)$$

Equations (7) and (8) can be transferred to (17) and (18) based on the d-q voltage frame.

$$E_d^* = E_{nom}^* - k_v(Q_{ref} - Q) + X_o\left(\frac{\omega_c}{s+\omega_c}\right)i_q \quad (19)$$

$$E_q^* = -X_o\left(\frac{\omega_c}{s+\omega_c}\right)i_d \quad (20)$$

ω_c : Cut-off frequency of low pass filter

It is possible to change (5), (7), and (18) to the small signal description as shown in from (19) to (21) (The error of the output and reference voltage is assumed as '0').

$$\triangle\omega = k_\omega \frac{\omega_c}{s+\omega_c}\triangle p \quad (21)$$

$$\triangle e_d = k_v \frac{\omega_c}{s+\omega_c}\triangle q + X_o \frac{\omega_c}{s+\omega_c}\triangle i_q \quad (22)$$

$$\triangle e_q = -X_o \frac{\omega_c}{s+\omega_c}\triangle i_d \quad (23)$$

The above equations are rewritten by replacing $\triangle\omega$ with $\triangle\phi$ and considering a low pass filter.

$$\triangle\ddot{\phi} + \omega_c\triangle\dot{\phi} = \omega_c k_\omega \triangle p \quad (24)$$

$$\triangle\dot{e}_d + \omega_c\triangle e_d = \omega_c k_v \triangle q + X_o\omega_c\triangle i_q \quad (25)$$

$$\triangle\dot{e}_q + \omega_c\triangle e_q = -X_o\omega_c\triangle i_d \quad (26)$$

Then (27) shows the phase of inverter ϕ, and (28) shows $\triangle e_q$.

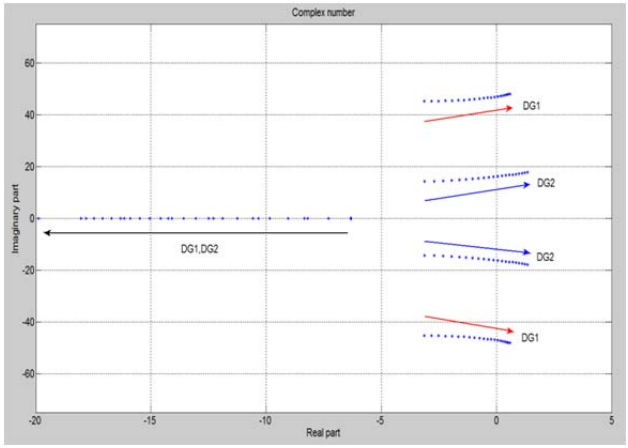

Fig. 7. System root locus with various X_o from 0 to 1.5mH.

$$\phi = \arctan\left(\frac{e_q}{e_d}\right) \quad (27)$$

$$\triangle e_q = \frac{e_d^2 + e_q^2}{e_d}\triangle\phi + \frac{e_q}{e_d}\triangle e_d \quad (28)$$

Finally, the state space equation matrix can be obtained as (29) from the above equations.

$$\begin{bmatrix} \triangle\dot{\phi} \\ \triangle\ddot{\phi} \\ \triangle\dot{e}_d \end{bmatrix} = \begin{bmatrix} 0 & 1 & 0 \\ a & -\omega_c & b \\ c & 0 & d \end{bmatrix}\begin{bmatrix} \triangle\phi \\ \triangle\dot{\phi} \\ \triangle e_d \end{bmatrix} \quad (29)$$

Where:

$$a = \frac{\omega_c k_\omega V}{Z}\sin\theta\frac{e_d^2 + e_q^2}{e_d}$$

$$b = \frac{\omega_c k_\omega V}{Z}\left(\cos\theta + \frac{e_q}{e_d}\sin\theta\right)$$

$$c = \cos\theta\frac{\omega_c(X_\circ - k_v V)}{Z}\frac{e_d^2 + e_q^2}{e_d}$$

$$d = -\omega_c + \frac{\omega_c(k_v V - X_\circ)\sin\theta}{Z} + \frac{\omega_c(X_\circ - k_v V)\cos\theta}{Z}\frac{e_q}{e_d}$$

Equation (29) can be expressed as $\triangle\dot{X} = AX$ and the system stability can be confirmed by using the value of $\triangle|sI - A| = 0$. Fig. 7 represents the Matlab simulation results based on (29) from the small signal modeling. Each parameter is same as the parameters for the simulation.

This represents the root locus for the eigenvalue of the state equation when the virtual inductance X_o changes from 0 to 1.5mH. As shown in this figure, one root moves to the left side and the other two roots move to the stable area on the right side. The stable area of the virtual inductance of DG1 is 0 to 0.265mH and it is 0 to 0.8mH for DG2. Therefore, the maximum virtual inductance can be selected as 0.265mH which satisfies both areas. Through this selected virtual inductance, the stability and effectiveness are satisfied

TABLE I
SIMULATION PARAMETERS OF DISTRIBUTED GENERATION SYSTEM FOR DROOP CONTROLLED PARALLEL INVERTERS

Parameters	Value
P_{ref}	100 [kW]
Q_{ref}	6.6 [kVar]
V_{dc}	158 [V]
Frequency droop k_ω	-1×10^{-5} [rad/W]
Voltage droop k_v	-1×10^{-7} [V/Var]
Filter capacitor C_f	2100 [uF]
Filter inductance L_f	15 [uH]
DG1 line impedance	0.02 [Ω], 0.08 [mH]
DG2 line impedance	0.15 [Ω], 0.17 [mH]
Switching frequency f_ω	8 [kHz]
Virtual inductance X_o	0.265 [mH]

simultaneously. The selected virtual inductance has also been adopted for the PSIM simulation.

III. SIMULATION

Table I shows the parameters of the parallel inverters for the simulation. The virtual inductance has been selected as 0.265mH from the small signal analysis. The line impedances are intentionally unbalanced and the line impedance of DG2 is assigned so that the resistive component is more predominant than the inductive component to validate the effect of the virtual inductor.

Fig. 8 represents the droop performances with two parallel inverters based on the virtual inductor method for three different types of conditions (a, b, c) and the conventional droop method using a high voltage droop coefficient with or without the ramp function at the transient state (d, e). The total simulation time is 2sec and the droop control is applied after 1sec. Fig. 8(a) shows the real and reactive powers, and the circulating current. Here, the unrated real power and reactive power sharing errors occur due to the high virtual impedance voltage drop and the unbalanced line impedances, respectively. Fig. 8(b) shows that the reactive power sharing error can be reduced after considering each voltage drop of the unbalanced line impedance [2]. The circulating current is also reduced to that of Fig. 8(a). However, the total value of the real power sharing is still smaller than the rated real power value. Fig. 8(c) adopts the voltage drop of the line impedances and the voltage drop of the virtual inductance based on (11). Compared with Fig. 8(b), Fig. 8(c) simultaneously achieves a reduction of the reactive power sharing error and the correct rated real power sharing. In addition, it is possible to use the high voltage droop coefficient instead of the line impedance voltage drop offset as shown in Fig. 8(d). However, its dynamic response

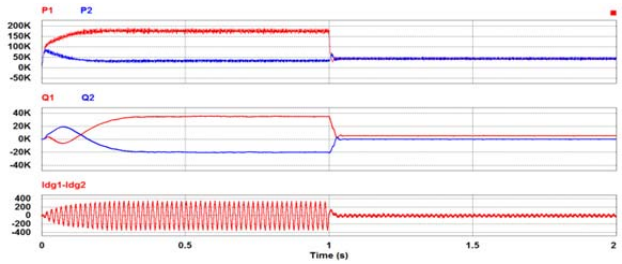

(a)

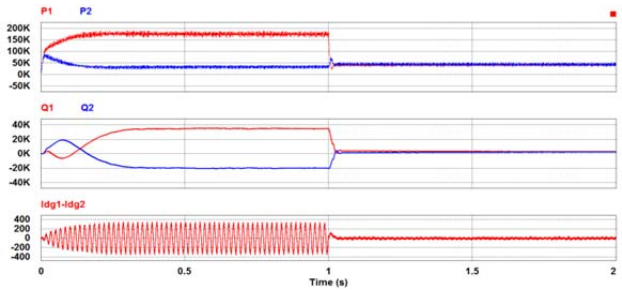

(b)

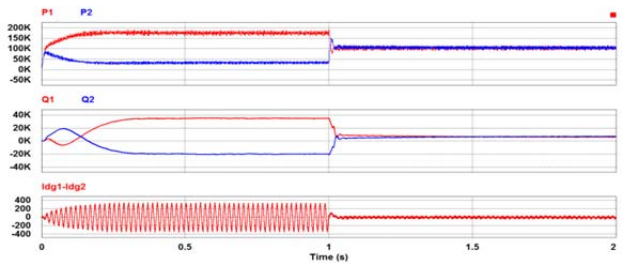

(c)

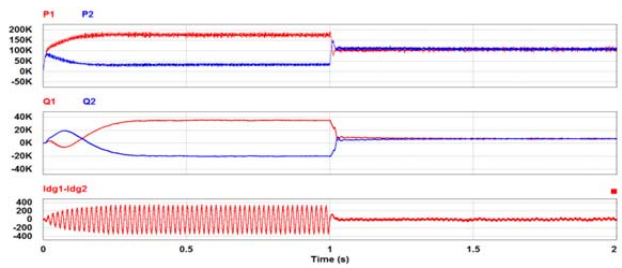

(d)

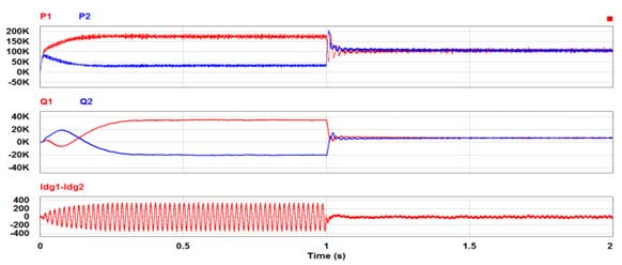

(e)

Fig. 8. Droop performances with two parallel inverters using virtual inductor method (top: active power, middle: reactive power, bottom: circulating current): (a) Conventional droop control considering equations (5) and (6), (b) droop control considering line impedance, (c) proposed droop control considering virtual inductance, (d) conventional droop control using high voltage droop gain, (e) conventional droop control using high voltage droop gain with ramp function in transient.

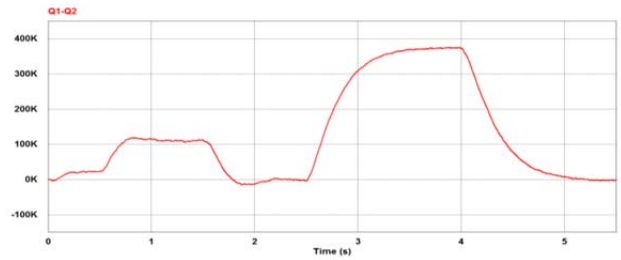

(a)

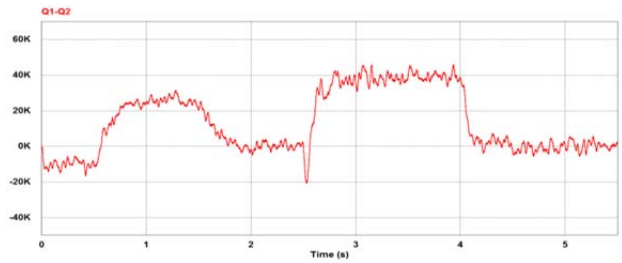

(b)

Fig. 9. Reactive power sharing errors under unequal line impedances with conventional droop control from 0.5 to 1.5sec and from 2.5 to 4sec and proposed droop control from 1.5 to 2.5sec and from 4 to 5.5sec: (a) Unequal line resistance and two times increase at 2.5sec, (b) unequal line inductance and two times increase at 2.5sec.

shows some oscillations which can be assumed to be unstable characteristics. Therefore, the ramp output of the voltage droop has been adopted in Fig. 8(e) to reduce the transient droop oscillation. However, although the dynamic response can be improved to be stable with the ramp function, the steady state oscillation still occurs due to the high voltage droop coefficient. Therefore, the proposed droop method considering the line impedance and virtual impedance voltage drop offset guarantees the correct real and reactive sharing performance and system stability in both the transient and steady states.

Fig. 9 represents the reactive power sharing error under different line impedance conditions. The conventional droop control is used during the periods of 0.5~1.5sec and 2.5~4sec. In addition, the proposed droop control is used during the periods of 1.5~2.5sec and 4~5.5sec. In Fig. 9(a), the line impedance of DG1 is 0.05 Ω and 0.08mH, and that of DG2 is 0.08 Ω and 0.08mH until 2.5sec. After that, the line resistance of DG2 becomes two times greater as 0.16 Ω to test the validity of the proposed droop performance in various line resistance conditions. In Fig. 9(b), the line impedance of DG1 is 0.05 Ω and 0.04mH, and that of DG2 is 0.05 Ω and 0.06mH until 2.5sec. After 2.5sec the line inductance of DG2 becomes two times greater as 0.12mH to test the validity of the proposed droop performance in various inductive line conditions. As shown in Fig. 9, there are reactive power sharing errors due to the unequal line impedances under the conventional drop method. However, the reactive power sharing error can be reduced by using the proposed droop

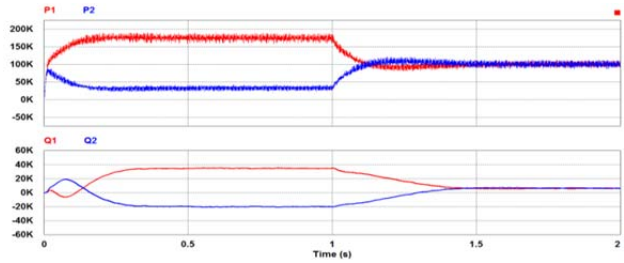

(a)

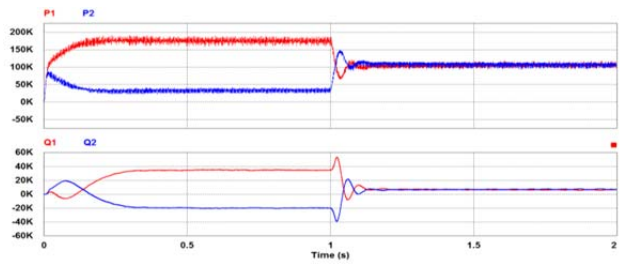

(b)

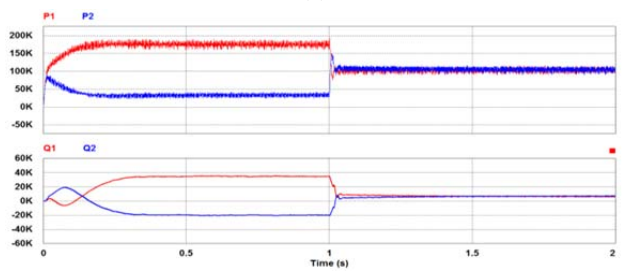

(c)

Fig. 10. Proposed droop performances with various virtual inductance (top: active power, bottom: reactive power): (a) Without X_o, (b) X_o = 0.07mH, (c) X_o = 0. 265mH.

method regardless of the various line impedances.

Fig. 10 represents the real and reactive powers when the proposed droop control is adopted with three different values for the virtual inductance. As in Fig. 8, the droop control and virtual inductor methods are applied at 1sec. The virtual inductance values are 0mH, 0.07mH, and 0.265mH in Figs. 10(a), 10(b), and 10(c), respectively. As shown in these figures, the larger virtual inductance value is, the faster and more correct the sharing of the real and reactive powers becomes. Note that an excessive increase of the virtual impedance which exceeds the right half plane on the root locus causes system instability.

Fig. 11 represents the droop performances of the real and reactive powers with the resistive droop (7) and (8) on a predominantly resistive line. Unlike Fig. 8(a), the reactive power sharing is correct, and the real power sharing error occurs in Fig. 11(a) due to the changed relation between the line component and the power flow. In addition, the unrated real power problem also remains same as in Fig. 8(a). Therefore, the line impedance voltage drop offset has been adopted in Fig. 11(b). However, the shared real powers are

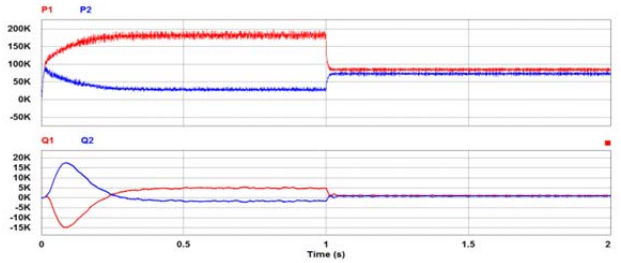

(a)

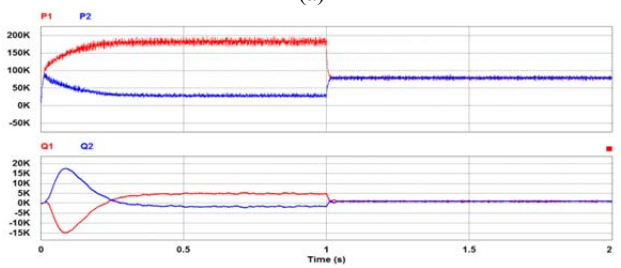

(b)

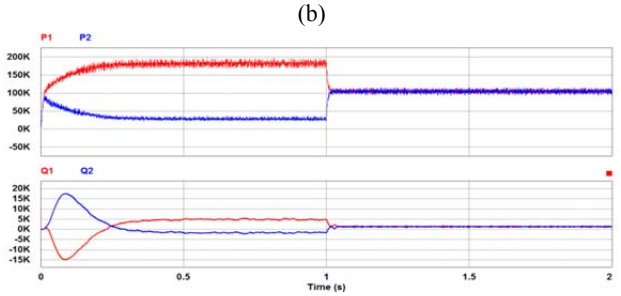

(c)

Fig. 11. Droop performance of real and reactive power with resistive droop equation (7) and (8) on resistive line (DG1: 0.03Ω and 0.008mH, DG2: 0.15Ω and 0.033mH): (a) Conventional resistive droop control, (b) resistive droop control considering only the line impedance, (c) proposed droop control considering full resistive (12).

still different from the rated value due to the high virtual impedance voltage drop. In Fig. 11(c), the resistive droop (12) has been fully adopted. As shown in these figures, the real and reactive power sharing error is almost zero and the real power rating is recovered to its rated value.

Fig. 12 represents the current waveforms under the proposed droop method with various virtual inductances. The virtual inductance value of each figure is 0, 0.265, 0.8mH. In the case of Fig. 12(b), its sharing dynamic response is faster and more correct than that of Fig. 12(a).

The virtual inductance of Fig. 12(c) is in the stable region of the small signal modeling of DG2. However, it is in the unstable region of the small signal modeling of DG1. That is why its current waveform is oscillating unstably. Hence, the validity of the small signal modeling in this paper is verified.

IV. Experimental Results

Table II represent the parameters of the droop control used for the experiments. As shown in Table II, the experimental setup is much lower scale than that of the simulation setup

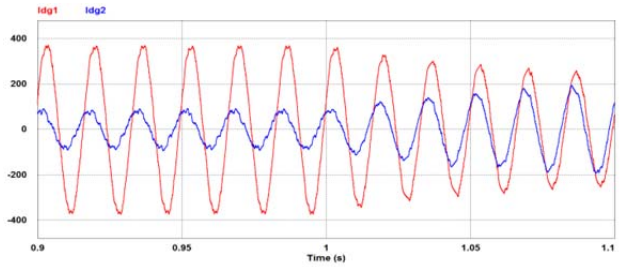

(a)

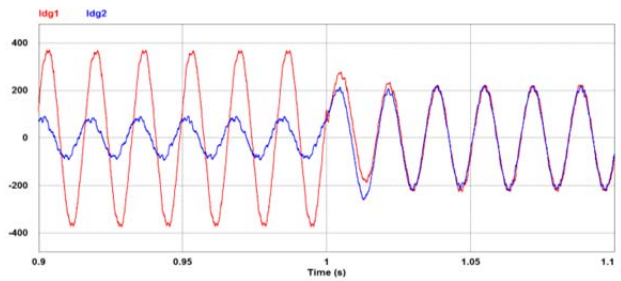

(b)

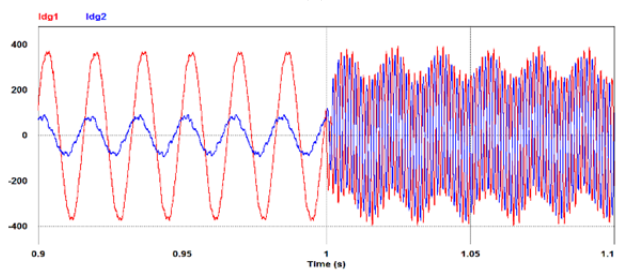

(c)

Fig. 12. Proposed droop performances with various virtual inductance (output current) (a) without Xo, (b) Xo=0.265mH, (c) Xo=0.8mH.

TABLE II
Experiment Parameters of Distributed Generation System for Droop Controlled Parallel Inverters

Parameters	Value
P_{ref} (case1)	800 [W]
Q_{ref} (case1)	35 [Var]
P_{ref} (case1)	460 [W]
Q_{ref} (case1)	26 [Var]
V_{dc}	190 [V]
Frequency droop k_ω	-1.5×10^{-4} [rad/W]
Voltage droop k_v	-1×10^{-6} [V/Var]
Filter capacitor C_f	100 [uF]
Filter inductance L_f	2 [mH]
DG1 line impedance	2 [Ω], 150 [uH]
DG2 line impedance	0.8 [Ω], 520 [uH]
Switching frequency f_ω	2,8 [kHz]
Virtual inductor X_o	8 [mH]
Virtual resistor R_o	1 [Ω]

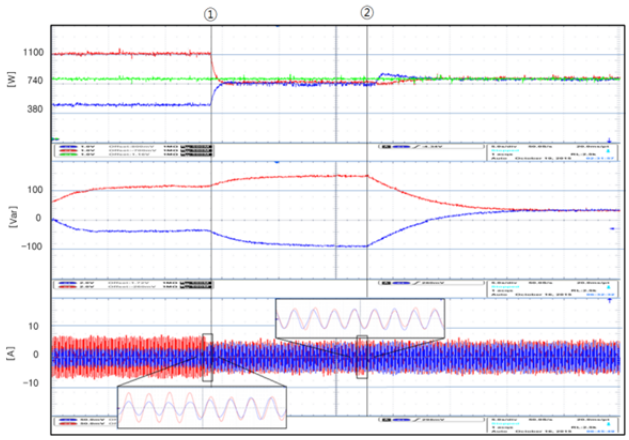

Fig. 13. Experimental results of droop performances with two parallel inverters using virtual inductor method (top: active power, middle: reactive power, bottom: output current).

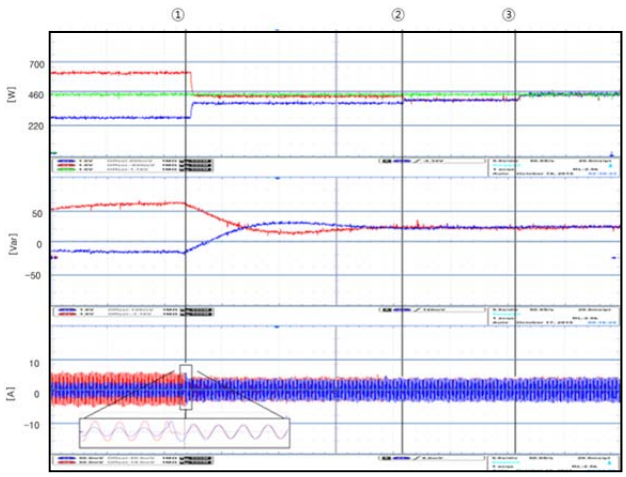

Fig. 14. Droop performances with two parallel inverters using virtual resistor method (top: active power, middle: reactive power, bottom: output current).

due to the power capacity of the laboratory.

Fig. 13 represents the droop performances using the virtual inductor method with two control transient characteristics. At ① in Fig. 13, the conventional droop control is started. Then, a reactive power sharing error occurred due to the unequal line impedance voltage drop. The real powers of two inverters are well shared but its shared power is reduced to less than its reference value due to the previously mentioned large virtual inductor voltage drop. Therefore, (11) is adopted at ② in Fig. 1 to reduce the reactive power sharing error and to change the unrated shared power to its rate value.

Fig. 14 represents the droop performances using the virtual resistor method with three control transient characteristics. At ① in Fig. 14, the conventional droop control is started. Then, a real power sharing error occurred although the reactive powers are not well shared when compared to the case of the virtual inductor. In addition, the real power does not satisfy its rated value. Therefore, at ② in Fig. 14, the line impedance voltage drop compensation is adopted to reduce the real power sharing error. As shown in (12), consideration of the virtual resistor effect has been implemented to change the real power to its rated value at ③ in Fig. 14. Each current waveform of the system shows the current sharing performances when the conventional or the proposed droop has been adopted. Finally, it is verified that the proposed droop method realizes the real and reactive power sharing along with the rated real power regulation.

V. CONCLUSION

The proposed droop method in this paper is based on a virtual impedance selected by a small signal stability analysis. Additionally, it has considered voltage drops at unequal line impedances which cause a reactive power sharing error as well as those at virtual impedances which cause a rated real power reduction. Consequently, the real and reactive power sharing can be properly realized. Hence, the circulating current of the inverter has also been minimized. Validation of the proposed droop method and virtual impedance selection have been provided by PSIM, MATLAB simulations and experimental results.

REFERENCES

[1] Jinwei He and Y. W. Li, "An Accurate Reactive Power Sharing Control Strategy for DG Units in a Microgrid," *IEEE, 8th International Conference on Power Electronics-ECCE Asia*, pp. 551-556, 2011.

[2] K. Lim and J. Choi, "Droop Control for Parallel Inverters in islanded microgrid considering unbalanced low-voltage line impedance," *Transactions of Korean Institute of Power Electronics(KIPE)*, Vol. 18, No. 4, pp. 387-396, Aug. 2013.

[3] X. Wang, J. M. Guerrero, F. Blaabjerg, and Z. Chen, "A review of power electronics based microgrids," *Journal of Power Electronics*, Vol. 12, No. 1, pp. 181-191, Jan. 2012.

[4] A. Tuladhar, K. Jin, T. Unger, and K. Mauch, "Parallel operation of single phase inverter modules with no control interconnections," in *Conf. Rec. of IEEE APEC97*, pp. 94-100, 1997.

[5] K. S. Parlak, M. Ozdemir, and M. T. Aydemir "Active and reactive power sharing and frequency restoration in a distributed power system consisting of two UPS units," *Electrical Power and Energy Systems*, Vol. 31,No. 5, pp. 220-226, Jun. 2009.

[6] K. D. Brabandere, B. Bolsens, J. V. Keybus, A. Woyte, J. Driesen, and R. A. Belmans, "A voltage and frequency droop control method for parallel inverters," *IEEE Trans. Power Electron.*, Vol. 22, No. 4, pp. 1107-1115, Jul. 2007.

[7] Y. Li and Y. W. Li, "Power management of inverter interfaced autonomous microgrid based on virtual frequency-voltage frame," *IEEE Trans. Smart Grid.*, Vol. 2, No. 1, pp. 30-40, Mar. 2011.

[8] J. Kim, H. Choi, and B. Cho, "A novel droop method for converter parallel operation," *IEEE Trans. Power Electron.*, Vol. 22, No. 1, pp. 25-32, Jan. 2002.

[9] Y. W. Li and C. N. Kao, "An accurate power control strategy for power-electronics-interfaced distributed

generation units operation in a low voltage multibus microgrid," *IEEE Trans. Power Electron*., Vol. 24, No. 12, pp. 2977-2988, Dec. 2009.
[10] W. Yao, M. Chen, J. Matas, J. M. Guerrero, and Z. M. Qian, "Design and analysis of the droop control method for parallel inverters considering the impact of the complex impedance on the power sharing," *IEEE Trans. on Ind. Electron*., Vol. 58, No. 2, pp. 576-588, Feb. 2011.
[11] K. Jung, K. Lim, D. Kim, and J. Choi, "Droop method for high-capacity parallel inverters in islanded mode using virtual inductor," *Transactions of Korean Institute of Power Electronics(KIPE)*, Vol. 20, No. 1, pp. 81-90, Feb. 2013.
[12] J. M. Guerrero, L. G. Vicuna, J. Matas, M. Castilla, and J. Miret, "Output impedance design of parallel- connected UPS inverters with wireless load-sharing control," *IEEE Trans. Ind. Electron*., Vol. 52, No. 4, pp. 1126-1135, Aug. 2005.
[13] Z. Guo, D. Sha, and X. Liao, "Wireless paralleled control strategy of three-phase inverter modules for islanding distributed generation systems," Journal of Power Electronics, Vol. 13, No. 3, pp. 479-486, May 2013.
[14] J. M. Guerrero, L. G. Vicuna, J. Matas, M. Castilla, and J. Miret, "A wireless controller to enhance dynamic performance of parallel inverters in distributed generation systems," *IEEE Trans. Power Electron*., Vol. 19, No. 5, pp. 1205-1213, Sep. 2004.
[15] J. He and Y. W. Li, "Analysis, design, and implementation of virtual impedance for power electronics interfaced distributed generation," *IEEE Trans. Ind. Appl*., Vol. 47, No. 6, pp. 2525-2538, Nov./Dec. 2011.
[16] K. Jung, K. Lim, D. Kim, and J. Choi, "Droop method for high-capacity parallel using virtual impedance," *9th International Conference on Power Electronics-ECCE Asia*, pp. 996-1002, 2015.
[17] K. Sao and P. W. Lehn, "Autonomous load sharing of voltage source converters," *IEEE Trans. Power Del.*, Vol. 20, No. 2, pp. 1009-1016, Apr. 2005.

Donghwan Kim was born in Cheongju, Korea. He received his B.S. degree from the School of Electrical Engineering, Chungbuk National University, Cheongju, Korea, in 2013. He is presently working towards his M.S. degree in the School of Electrical Engineering, Chungbuk National University.

Kyosun Jung was born in Cheongju, Korea. He received his B.S. and M.S. degrees from the School of Electrical Engineering, Chungbuk National University, Cheongju, Korea, in 2013 and 2015, respectively. His current research interests include the load sharing of DG based microgrids and system stability analysis.

Kyungbae Lim was born in Cheongju, Korea. He received his B.S. and M.S. degrees from the School of Electrical Engineering, Chungbuk National University, Cheongju, Korea, in 2011 and 2013, respectively, where he is presently working towards his Ph.D. degree. His current research interests include harmonic compensation and seamless mode transfer in microgrids.

Jaeho Choi received his B.S., M.S., and Ph.D. degrees from the Department of Electrical Engineering, Seoul National University, Seoul, Korea, in 1979, 1981, and 1989, respectively. From 1981 to 1983, he was with the Jungkyoung Technical College, Daejeon, Korea, as a full-time Lecturer. Since 1983, he has been with the School of Electrical Engineering, Chungbuk National University, Cheongju, Korea, where he is presently a Professor. In 1993, 1998, 2003, and 2009 he was a Visiting Professor at the University of Toronto, Toronto, Canada. He was also a Danfoss Visiting Professor at Aalborg University, Aalborg, Denmark, in 2000. His current research interests include power electronics, power quality problems and solutions, energy storage systems, and renewable energy and microgrid systems. He is an active Member of the KIEE, KIPE, and IEEE. He was the Editor-in-Chief of the JPE and the President of the KIPE.